RESEARCH PAPER

Hydrogel-Based Nanocomposite Photocatalyst Containing In_2S_3/ g-C_3N_4 for Removal of Dye from Water

Janan Parhizkar[1,*], Mohammad Reza Mohammad Shafiee[2]

[1] Nanotechnology Laboratory, Department of Chemistry, University of Isfahan, Isfahan, Iran

[2] Department of Chemistry Faculty of Sciences, Islamic Azad University– Najafabad Branch, Najafabad, Iran.

ARTICLE INFO

Article History:
Received 27 June 2020
Accepted 11 September 2020
Published 15 October 2020

Keywords:
g-C_3N_4
In2S3
Heterojunction photocatalyst
Resorcinol formaldehyde hydrogel

ABSTRACT

A novel resorcinol formaldehyde hydrogel-based matrix was synthesized to stabilize indium sulfide / graphitic carbon nitride (In_2S_3/ g-$C_3N_{4)}$ heterojunction, and the adsorption performance and photocatalytic degradation activity of RhB over In_2S_3/ g-C_3N_4 in hydrogel were explored. The g-C_3N_4 nanosheets and In_2S_3 nanoparticles were synthesized and characterized by Fourier-transform infrared spectroscopy (FTIR), and UV-Vis diffuse reflectance spectroscopy (DRS). In_2S_3 and g-C_3N_4 were stabilized in hydrogel, and In_2S_3/ g-C_3N_4 in hydrogel was characterized by FFIR, DRS, X-ray diffraction, Brunauer-Emmett-Teller (BET) surface area analysiand Barrett-Joyner-Halenda (BJH) pore volume and pore size analysis, field emission scanning electron microscopy, and energy dispersive X-ray. The measured bandgap for In_2S_3/ g-C_3N_4 in hydrogel was 2.1 eV. BET results showed that the presence of heterojunction in the synthesis process of hydrogel dramatically increases the specific surface area about 20 times. In_2S_3/ g-C_3N_4 in hydrogel adsorbed RhB (25 ml of 3 ppm solution) about 72% and removed RhB under light irradiation about 89% in 120 min. The RhB removal reactions over In_2S_3/ g-C_3N_4 in hydrogel in both dark and under light irradiation conditions follow the first-order kinetic. This study reveals a new potential application of resorcinol formaldehyde hydrogel as a porous matrix to stabilize nano-size photocatalysts.

How to cite this article
Parhizkar J., Mohammad Shafiee M.R. Hydrogel-Based Nanocomposite Photocatalyst Containing In_2S_3/ g-C_3N_4 for Removal of Dye from Water. Nanochem Res, 2020; 5(2):168-178. DOI: 10.22036/ncr.2020.02.007

INTRODUCTION

In recent years, the development of efficient semiconductor photocatalyst working under visible light for various photo-dependent applications has become as a hot research topic. Photocatalytic semiconductors can solve two serious issues in 21st century, energy and environment [1].

Dyes and pigments in industrial wastewaters due to their non-biodegradable structure and toxic nature are harmful for the human health and cause lots of environmental hazards. Advanced oxidation process by photocatalysts can overcome the limitations of conventional methods employed for decomposition of organic dyes in polluted waters [2]. Photocatalysis is a promising candidate for environmental purification because of its advantages including nontoxicity, cheapness, and mild condition reaction.

Despite the appreciable developments of photocatalytic technology, its commercial application is significantly restricted due to the fast recombination of electron-hole pair and wide bang-gap of photocatalyst leading to activation of photocatalyst only under UV light irradiation [3]. Thus, numerous efforts have been devoted to fabricate the semiconductor system with a narrow bandgap and delayed recombination of electron-hole pair.

The graphite-like carbon nitride (g-C_3N_4), as a shining star in the photocatalytic field, possesses

* Corresponding Author Email: *jananparhizkar@gmail.com*

many unique properties, including high thermal, chemical, and photochemical stability, suitable band position, and low price [4, 5]. It is a metal-free two-dimensional polymer composed of a layered sheet of C and N covalently bonded in the form of a tris-triazine ring structure with a high degree in condensation [6]. The pure g-C_3N_4 suffers from disadvantages, including deficient sunlight absorption and high recombination rate of electron-hole pairs that affect its photocatalytic activity under visible light irradiation, notwithstanding the benefits of g-C_3N_4 [7].

One of the effective ways to modify g-C_3N_4 to improve catalytic performance is using heterojunction structure. Different semiconductors were integrated with g-C_3N_4 such as Ag_3VO_4 [8], AgX [9], $Ni_xCo_{1-x}S_2$ [10], WO_3 [11], MoS_2 [12], and In_2S_3 [13, 14].

In_2S_3 is a narrow bandgap n-type semiconductor having three different forms including α, β, and γ- In_2S_3. β- In_2S_3 with strong visible light absorption, suitable band potential, high photoconductivity, stable chemical and physical characteristics, and low toxicity attracts much attention in photocatalysis [13-17].

The high conductivity and mobility of charge carriers lead to the withdraw of photo-generated electrons from g-C_3N_4. The high conductivity of β-In_2S_3 nanoparticles integrated with g-C_3N_4 helps to efficient charge transport and improves the photocatalysis performance [14].

Research findings exhibit that enhanced visible light absorption and improved separation of electrons and holes in In_2S_3/ g-C_3N_4 nanocomposites lead to better photodegradation of RhB [18]. Kokane et al. reported that the photocatalytic activity of In_2S_3/ g-C_3N_4 composite for degradation of both cationic and ionic dyes was the same. Also, their studies revealed that light absorption and lifetime of photogenerated charge carriers are enhanced in this system [14].

Despite the efficient photocatalytic performance of In_2S_3/ g-C_3N_4 nanocomposite in dye degradation, its separation from reaction media and recycling limits its application in practical situations. To overcome this problem, the immobilization of catalysts in the suitable substrate can provide promising conditions including easy removal of catalyst without cost and time-consuming process, convenient reuse of catalyst, and unpolluted reaction medium by nanomaterials. Hydrogel as a three-dimensional porous structure can have an appealing potential application to serve as a substrate. They can be used as a desirable candidate for supporting nanocomposite due to their unique intrinsic properties such as porous network which leads to rapid mass transport, their large accessible surface area for adsorption and photoreaction, and inhibition of nanomaterials aggregation and prevention of efficiency decreasing [19-22].

Herein, we selected resorcinol formaldehyde hydrogel (RFH) obtained from the polycondensation of resorcinol with formaldehyde under alkaline condition. The covalent crosslinking of these clusters creates a 3D framework with a functionalized surface. The RFH is red dark [23].

In this study, we synthesized g-C_3N_4 and In_2S_3 semiconductors and then immobilized them into a RFH as a porous substrate. The main advantage of In_2S_3/ g-C_3N_4 in hydrogel composite was using a combination of visible light absorption and increased lifetime of electrons and holes provided by the heterojunction structure of In_2S_3/ g-C_3N_4 with rapid mass transport and easy recycling of catalyst provided by hydrogel as a substrate to obtain high-performance photocatalyst for dye removal from water.

EXPERIMENTS

The reagents used in the experiment were of analytical grade and used without any further purification. Indium (III) chloride ($InCl_3$), melamine ($C_3H_6N_6$), sodium sulfide nonahydrate ($Na_2S_3.9H_2O$), RhB (C.I.45170), resorcinol ($C_6H_6O_2$), formaldehyde (CH_2O), and sodium carbonate (Na_2CO_3) were analytically pure and from sigma Aldrich Co.

Synthesis of samples

In_2S_3 nanoparticles were synthesized by a simple precipitation method.

First, 0.01 M $InCl_3$ ethanol-water solution (1:1 v/v) was prepared. 0.03 M Na_2S solution in the ethanol-water mixture (1:1 v/v) was prepared and slowly added to the InCl3 solution under constant stirring and kept for 2 h. The mixture was centrifuged and precipitate was washed three times with distilled water and ethanol and then dried at 120 ^oC for 12 h. Ethanol was served as a solvent due to make dispersing medium and preventing agglomeration during the growth process [14, 24].

To obtain graphitic carbon nitride (g-C_3N_4), 10 g of melamine was placed into a semi-closed combustion boat, which heated at a rate of 5 C min^{-1}

to reach 600 °C and then was kept at this temperature for 2 h under ambient condition [19, 25].

Resorcinol formaldehyde (RF) hydrogel was made by polycondensation of resorcinol and formaldehyde in the presence of Na_2Co_3 as the catalyst. Resorcinol and Na_2CO_3 (R/C=300) were mixed and then dissolved in distilled water. The solution was heated to 70 °C under magnetic stirring in a sealed flask. In another flask, formaldehyde (37 wt. % in Water, stabilized by 10-15 wt. % Methanol) was heated to 70 °C. The solutions of the two mentioned flasks were mixed. The solution divided equally into sample holders with diameter and height equal to 13 and 20 mm, respectively. Then, each sample holder was sealed with paraffin film and solutions were put in an oven at 70 °C for 120 min [26].

To synthesize In_2S_3/ g-C_3N_4 stabilized in hydrogel, 10 mg of In_2S_3 nanoparticles and 5 mg of g-C_3N_4 per 1 ml of RF were added and the mixture was stirred for 4 min, and after casting in sample holders they were put in an oven at 70 °C for 120 min.

Characterization

The phase purity and crystal structure of the sample were recorded by x-ray diffraction (XRD) measured on a D8 Advance, BRUKER with a Cu anode in 2θ=5-80°. The surface morphology and nanostructure of the samples were observed with a field emission scanning electron microscope (FESEM, scientific England Agar Company). The specific surface area (BET), pore volume, and size were recorded at 77 K using apparatus BEIOSORP Mini from Microtrac Bel Crop. Diffuse reflectance spectra (DRS) were recorded using a V-670, JASCO spectrophotometer in the range of 200-900 nm and transformed to the absorption spectra according to the Tauc relationship. The infrared spectra were obtained on a FT-IR 6300 using KBr as the reference sample within a wavelength range of 400 – 4000 cm^{-1}.

Photocatalytic removal of RhB

3 ppm of RhB solution was selected as polluted water to investigate the photocatalytic performance of the catalyst. The hydrogel was put in 25 ml of 3 ppm RhB solution in a petri dish while stirring the solution in a dark condition. Every 10 min, the catalyst was removed from the solution and the concentration of RhB was monitored by a UV-Vis spectrophotometer till 120 min. Also, this progress was done under visible light irradiation. The results in dark condition reveal the absorption capacity of In_2S_3/ g-C_3N_4 stabilized in hydrogel and the obtained results under light exposure demonstrate the photocatalytic performance of the abovementioned catalyst.

RESULTS AND DISCUSSION

Fig.1 shows the FTIR spectra of the hydrogel, g-C_3N_4, In_2S_3 nanoparticle, and In_2S_3/ g-C_3N_4 in hydrogel. In FTIR spectrum of the hydrogel, the broad absorption band at 3428 cm^{-1} is attributed to hydroxyl groups bonded to the benzene rings. The stretching vibrations of CH_2 were observed at 2938 cm^{-1} and 1469 cm^{-1}. The band at 1608 cm^{-1} is related to aromatic ring stretching. The bands at 1087 cm^{-1} and 1290 cm^{-1} can be attributed to the formation of the C-O-C bond due to polycondensation reaction between resorcinol and formaldehyde [19].

In FTIR spectrum of g-C_3N_4, the peak at 1641 cm^{-1} is related to C=N stretching vibrations mode. The peaks at 1237 cm^{-1}, 1317 cm^{-1}, and 1466 cm^{-1} are assigned to aromatic C-N stretching vibration modes [27]. The sharp absorption peak at 809 cm^{-1} is attributed to the breathing vibration of the tri-s-triazine cycle[28]. The characteristic peak in FTIR spectrum of In_2S_3 nanoparticles is observed at 807 cm^{-1} due to bonding of In-S [29]. The peak at 477 cm^{-1} is related to formation of Na_2S during synthesis of In_2S_3. The intense peak at 3354 cm^{-1} is due to adsorbed water molecules on the surface of samples.The peak at 1605 $cm^{-1}$is related to C=O stretching vibration of adsorbed CO_2 molecules [30]. The FTIR spectrum of In_2S_3/ g-C_3N_4 stabilized in hydrogel is very similar to that of hydrogel because of small amounts of In_2S_3 and g-C_3N_4.

The crystal structure of the composite was examined by XRD. Fig.2 shows the XRD pattern of In_2S_3/ g-C_3N_4 in hydrogel. As shown in Fig.2, the composite has an amorphous phase that can be attributed to the hydrogel. The sharp peak at 44° matches with the most intensive peak of carbon with JCPDS.no 01-075-0409 (diamond). This peak probably confirms the crystalization of carbon in the hydrogel. The characteristic peaks of pure g-C_3N_4 and In_2S_3 are not observed at the XRD spectrum because of the small amount of these materials in comparison with hydrogel.

The optical properties of g-C_3N_4, In_2S_3 nanoparticle, and In_2S_3/ g-C_3N_4 in hydrogel were investigated using UV–Vis diffuse reflectance spectroscopy. The optical absorption spectra of g-C_3N_4, In_2S_3 nanoparticle, and In_2S_3/ g-C_3N_4 in hydrogel are

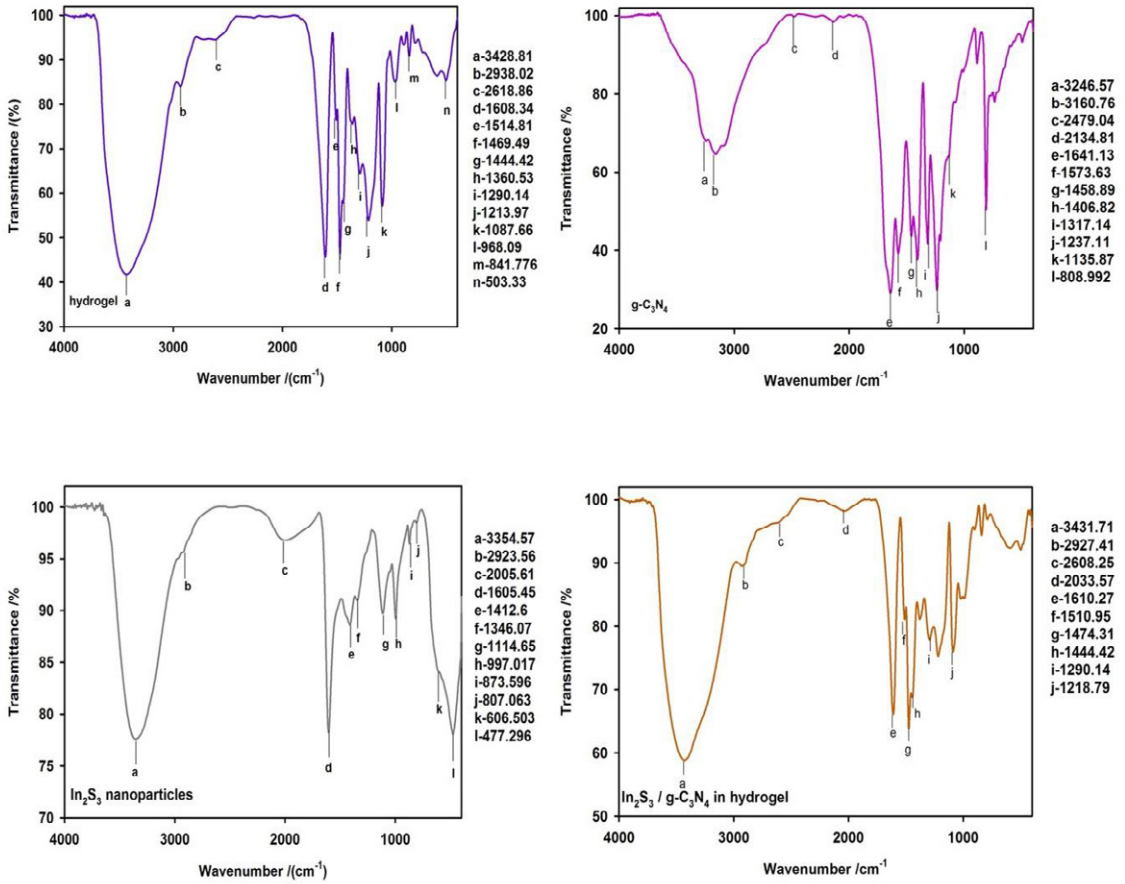

Fig. 1. FTIR spectra of hydrogel, g-C_3N_4, In_2S_3 nanoparticles, and In_2S_3/ g-C_3N_4 in hydrogel.

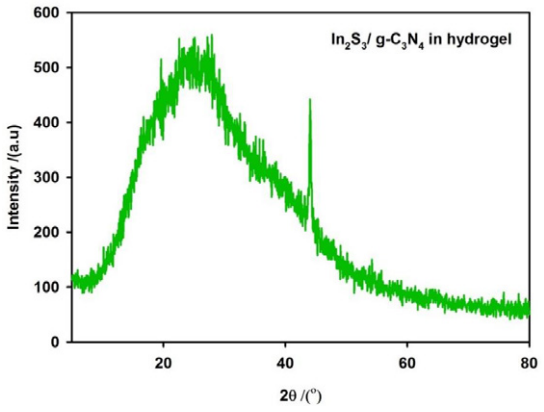

Fig. 2. XRD pattern of In_2S_3/ g-C_3N_4 in hydrogel.

shown in Fig. 3. The increased absorption edges of g-C_3N_4 and In_2S_3 were observed at 460 and 500 nm, respectively. The absorption edge of In_2S_3/ g-C_3N_4 heterojunction stabilized in hydrogel shifted to longer wavelength (about 700 nm) in comparison with g-C_3N_4 and In_2S_3, implying that this composite works with visible light [18, 14]. The optical band gap of g-C_3N_4, In_2S_3, and In_2S_3/ g-C_3N_4 in hydrogel were calculated using Tauc relation $\alpha h\nu=A(h\nu-E_g)^n$ where α is the absorption coefficient. A, ν, E_g, and

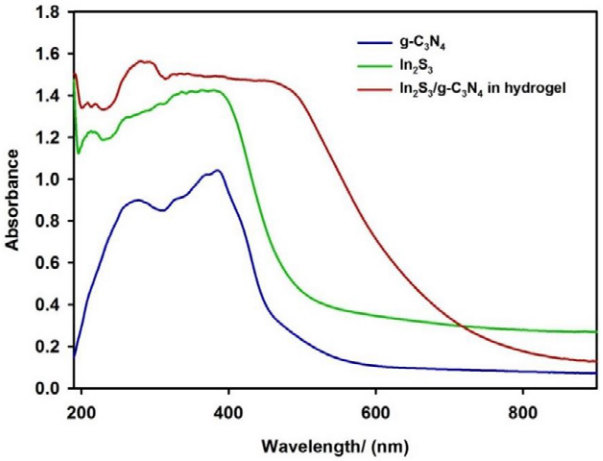

Fig. 3. UV–Vis DRS absorbance spectra of g-C_3N_4, In_2S_3 nanoparticle, and In_2S_3/ g-C_3N_4 in hydrogel

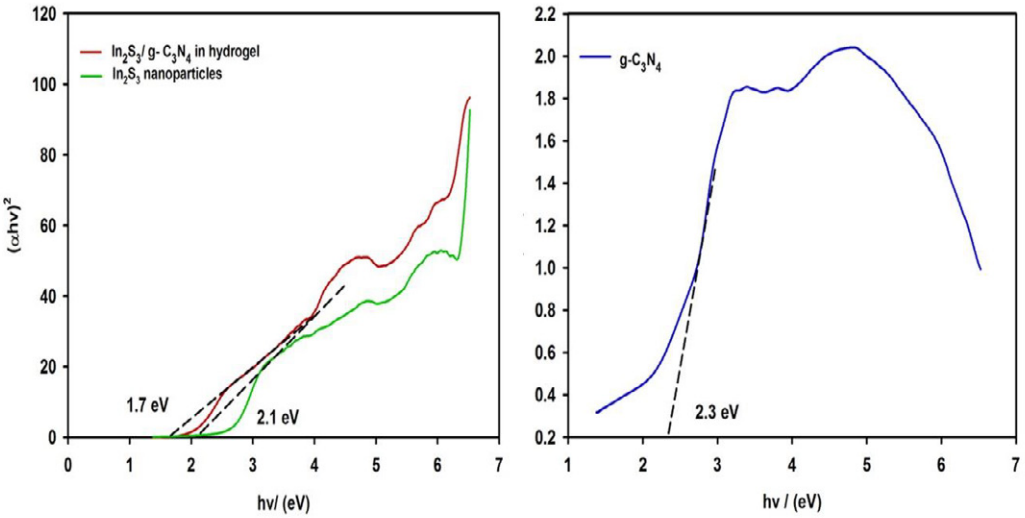

Fig. 4. Tauc plots of g-C_3N_4, In_2S_3 nanoparticle, and In_2S_3/ g-C_3N_4 in hydrogel

n are constant, light frequency, bandgap, and an index, respectively. The n value is determined by different typical optical transitions of the semiconductor (n= 1/2 for a direct transition and n=2 for an indirect transition)[31]. In_2S_3 is a direct transition semiconductor and its bandgap (E_g) was obtained from a plot of $(\alpha h\nu)^2$ vs hν. The measured band gap was found to be 1.7 eV for In_2S_3. g-C_3N_4 is an indirect semiconductor and its E_g was obtained by an extrapolation of the linear range of plot $(\alpha h\nu)^{1/2}$ vs hν about 2.3 eV. Because of the more amounts of In_2S_3 rather than g-C_3N_4 in heterojunction, the In_2S_3/ g-C_3N_4 in hydrogel is accounted as a direct bandgap semiconductor and the measured bandgap was about 2.1. The measured band gap of g-C_3N_4 in this research differs from reported values by others. Also, the bandgap of In_2S_3/ g-C_3N_4 is lower than the obtained bandgap of this heterojunction reported by Kokane et al (2.66 eV)[14]. This smaller bandgap can be attributed to two reasons:

- The smaller bandgap of our g-C_3N_4 in comparison with the bandgap of g-C_3N_4 reported in the literature.
- Presence of hydrogel with a high oxygen content which has interaction with heterostructure.

The hydrogels are porous materials. The technique of N_2 adsorption-desorption isotherms was used to evaluate the surface area and porosity type. Fig 5 shows the isotherms of hydrogel and In_2S_3/ g-C_3N_4 in the hydrogel. The isotherms are type IV that imply the mesoporous nature of materials. The shapes of the hysteresis loop confirm that pores

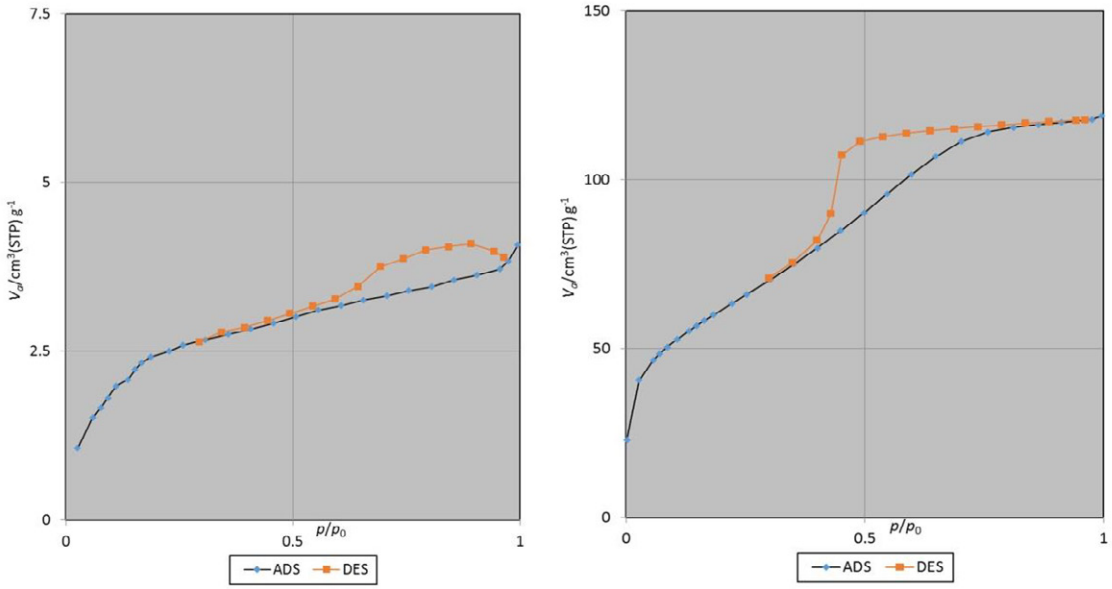

Fig. 5. N_2 adsorption-desorption isotherms of hydrogel (left), and In_2S_3/ g-C_3N_4 in hydrogel (right)

Table 1 Specific surface area, pore volume and pore diameter of the hydrogel, and In_2S_3/ g-C_3N_4 in hydrogel

Sample	S_{BET} ($m^2.g^{-1}$)	Pore volume ($cm^3.g^{-1}$)	Mostly pore diameter By BJH (nm)
Hydrogel	10.066	0.0040829	2.52
In_2S_3/g-C_3N_4 in hydrogel	219.69	0.144	3.92

have a bottleneck shape. The specific surface area, pore-volume, and pore size of samples were investigated by BET and BJH, respectively. The BET surface area of the hydrogel is 10.066 $m^2.g^{-1}$ while the BET surface area of In_2S_3/ g-C_3N_4 in the hydrogel is 219.69 $m^2.g^{-1}$. It can be seen clearly from BET results that the addition of In_2S_3 and g-C_3N_4 to hydrogel not only does not decrease the porosity but also increases surface area about twenty times. The pore volumes of hydrogel and In_2S_3/ g-C_3N_4 in the hydrogel were obtained 0.00408 and 0.144 $cm^3.g^{-1}$, respectively. The most probable pore diameters for the above-mentioned samples measured by BJH were between 2.52 and 3.92 nm. BJH measurements confirm that the presence of nanomaterials enhances the pore diameter and pore volumes. It can be concluded that RFH has an amazing structure to stabilize the catalysts without losing its porosity. The BET and BJH results are tabulated in Table 1

To characterize the morphology of the hydrogel and In_2S_3/ g-C_3N_4 in the hydrogel, FESEM was performed as shown in Fig .6. The samples have a uniform grainy and porous structure. The size distributions are relatively narrow. The particles in hydrogel have an average diameter of about 12.25 nm. The pores have a diameter between 16.00 nm and 19.18 nm. The particles in In_2S_3/ g-C_3N_4 in hydrogel have a diameter from 19.04 to 28.55 nm. The EDX spectrum of In_2S_3/ g-C_3N_4 in hydrogel confirms the presence of C, N, In and S elements (Fig.7).

Dye removal

The removal activity of hydrogel and In_2S_3/ g-C_3N_4 in hydrogel was evaluated by the removal of 3 ppm of RhB under dark condition (adsorption) and visible light irradiation (synergy of adsorption and photocatalysis). The results are shown in Fig. 8 based on the plot of C_t/C_0 versus time (t), where C_t is the concentration of RhB at the time t, and C_0 is the initial concentration of RhB solution. As Fig. 8 shows, pure hydrogel has a low capacity to adsorb RhB from solution but by addition g-C_3N_4 and In_2S_3 to hydrogel the adsorption capacity increases severely. This can be due to the presence of g-C_3N_4 and In_2S_3 nanomaterials with high active surfaces for interaction with dye, and also, the enhancement of hydrogel porosity which improves mass transfer

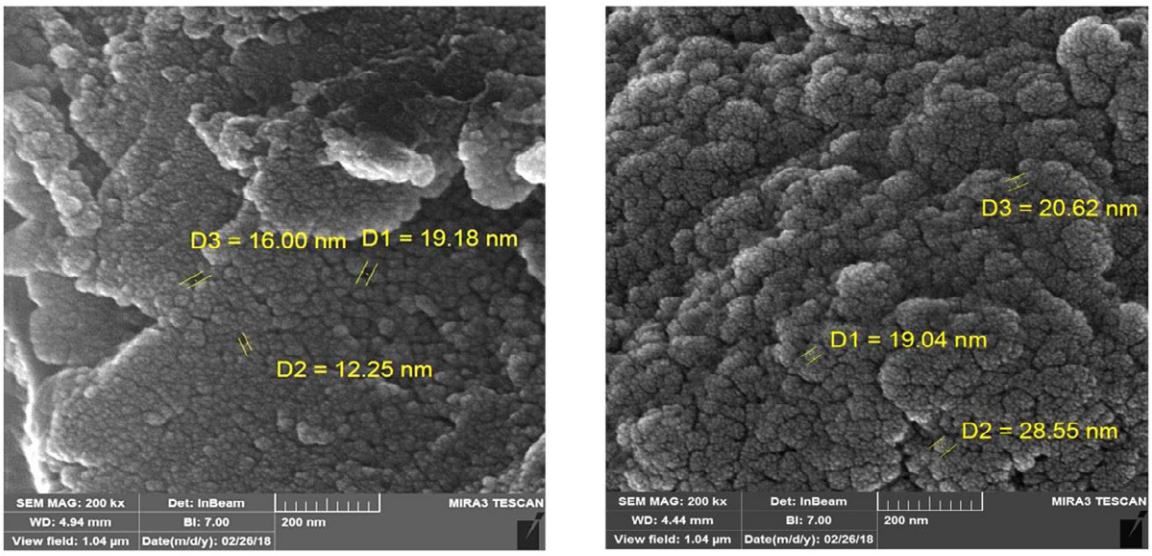

Fig. 6. FESEM image of hydrogel (left) and In_2S_3/ g-C_3N_4 in hydrogel (right)

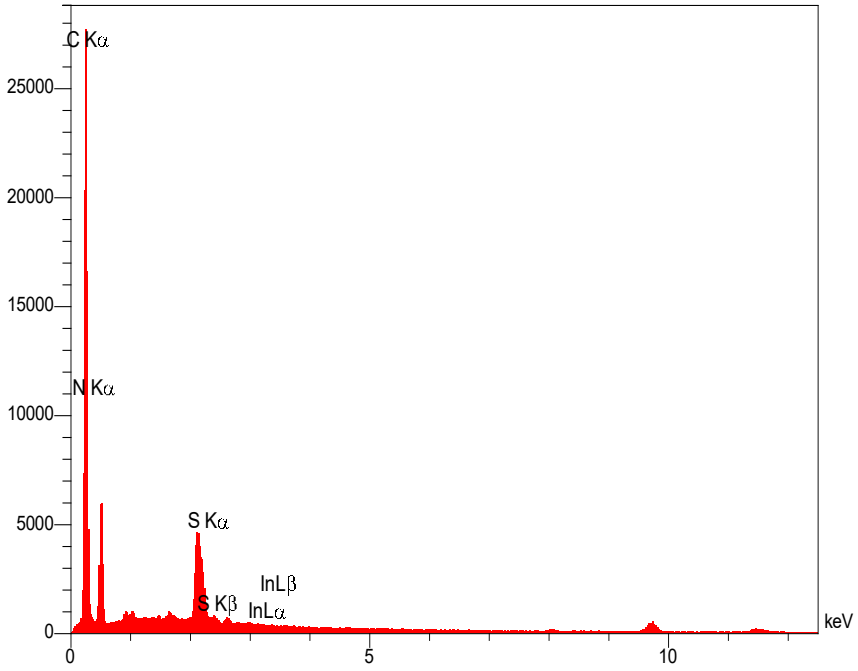

Fig. 7. EDX spectrum of In_2S_3/ g-C_3N_4 in hydrogel

in hydrogel and expands effective interaction surfaces. The removal of RhB under light irradiation which includes adsorption and photocatalysis processes is higher than the removal only by adsorption. Fig .9 shows the removal percentages of hydrogel and In_2S_3/ g-C_3N_4 in hydrogel. After 120 min in dark condition hydrogel only adsorbs 7% of RhB while In_2S_3/ g-C_3N_4 in hydrogel can adsorb about 72% of dye in solution. Under light exposure, In_2S_3/ g-C_3N_4 in hydrogel removes RhB about 88.6%. It means that the contribution of photocatalysis in dye removal is equal to 16.8%. The RhB removal performance of In_2S_3/ g-C_3N_4 in hydrogel is compared with reported amounts of In_2S_3/ g-C_3N_4 in

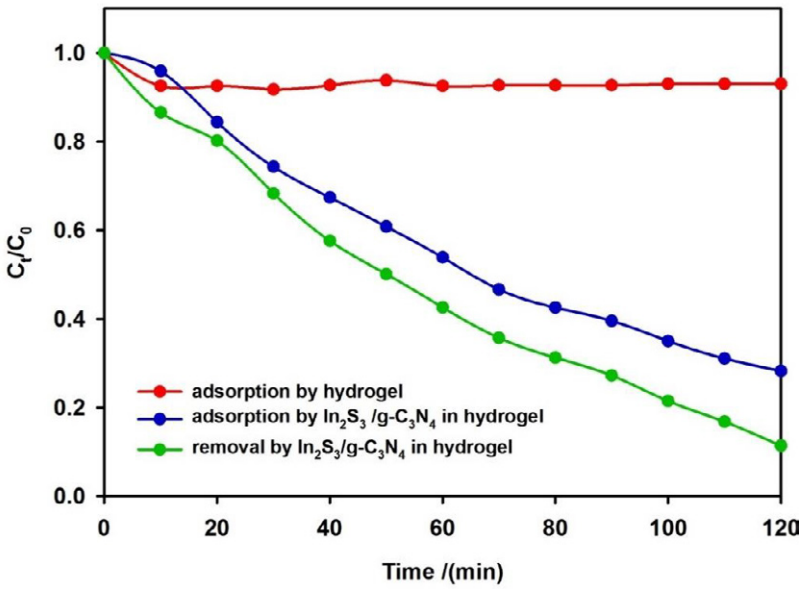

Fig. 8. Relative concentration of RhB over hydrogel and In_2S_3/ g-C_3N_4 in hydrogel in dark condition and under light irradiation.

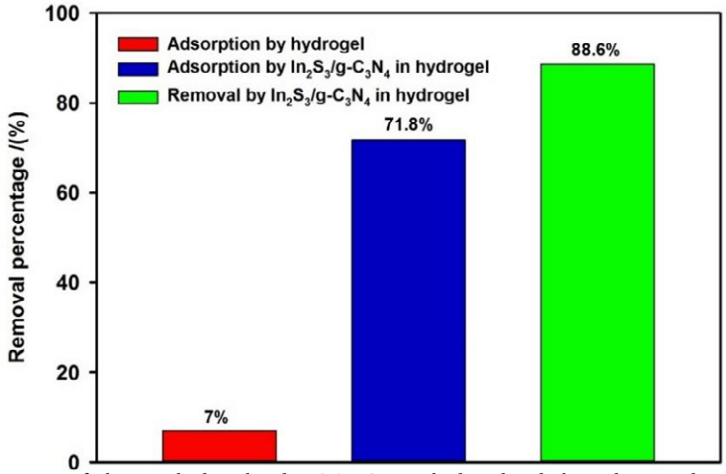

Fig. 9 Removal percentages of RhB over hydrogel and In_2S_3/ g-C_3N_4 in hydrogel in dark condition and under light irradiation.

Table 2. Comparison of In2S3/ g-C3N4 performances for RhB removal

Sample	Amount of Heterostructure	Time	C_0 dye solution	Solution Volume	Removal %
30-70% In_2S_3/ g-C_3N_4 [11]	50 mg	30 min	10 mg/L	50 ml	56-96%
25%In_2S_3/g-C_3N_4 [17]	100 mg	225min	5×10^{-5} M	100ml	>90%
In_2S_3/ g-C_3N_4 in hydrogel	<25 mg	120 min	3 mg/L	25 ml	88.6%

publications in Table 2. It can be seen from Table 2 that the immobilization of heterostructure in hydrogel has no considerable effect on the removal performance of In_2S_3/ g-C_3N_4. Also, the stabilization of heterostructure in hydrogel facilitates the exit of catalyst from reaction media without any further treatment to remove the catalyst from the aqueous solution.

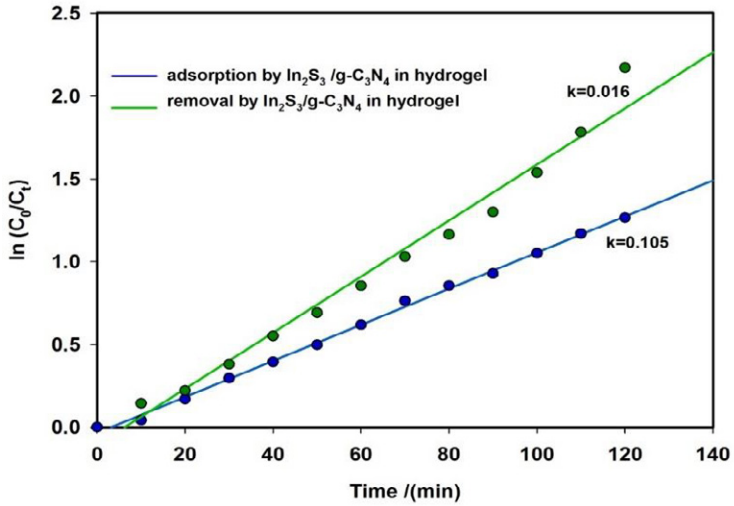

Fig. 10. The removal kinetics of RhB over In_2S_3/ g-C_3N_4 in hydrogel in dark condition (adsorption) and under light irradiation (removal).

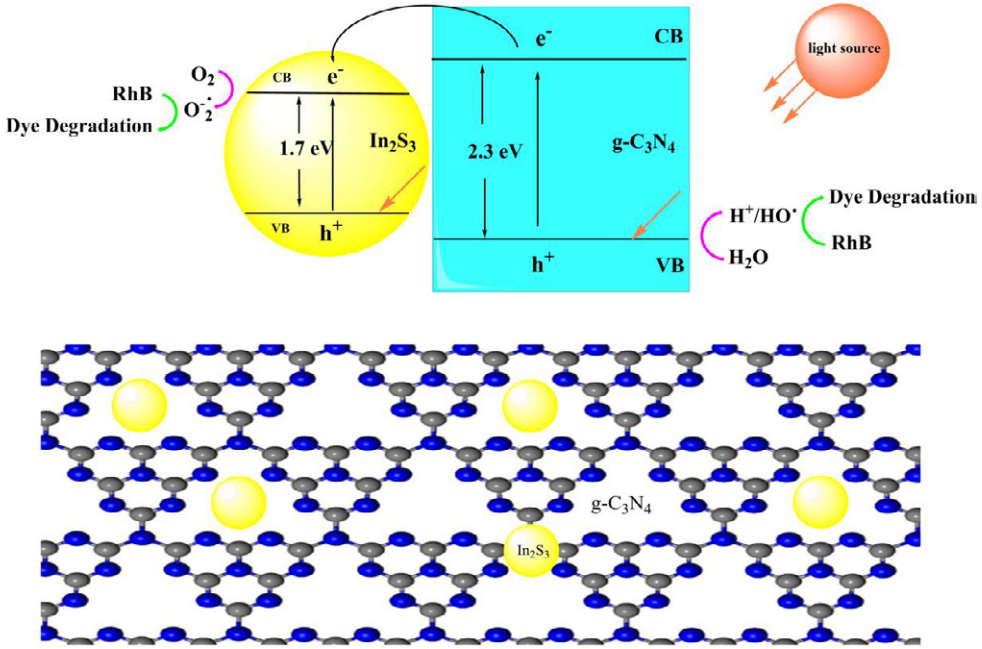

Fig. 11. Schematic illustration of the In_2S_3/ g-C_3N_4 photodegradation process under visible light irradiation.

The adsorption and photodegradation of organic pollutants follow the firs order kinetic as is given below:

$$\ln \frac{C_0}{C_t} = Kt$$

where C_0 is initial RhB concentration (ppm), C_t is RhB concentration at time t (ppm), and K is the first-order kinetic constant (min^{-1}). Fig.10 displays the linear relationship between ln (C_0/ C_t) and time for RhB removal using In_2S_3/ g-C_3N_4 in hydrogel in dark condition and under light irradiation. The K value for RhB adsorption over hydrogel In_2S_3/ g-C_3N_4 in hydrogel is 0.0105 min^{-1} (R^2=0.99) while under light irradiation it will reach 0.016 min^{-1} (R^2= 0.97).

Fig. 11 exhibits the schematic of photocata-

lytic degradation of RhB in the presence of In_2S_3/ g-C_3N_4 in hydrogel. Probably under light irradiation, In_2S_3 and g-C_3N_4 are excited, and subsequently, electron-hole pairs are generated. The electrons in the conduction band of g-C_3N_4 are transited to the conduction band of In_2S_3. Then, the risk of electron-hole recombination in g-C_3N_4 decreases and the effective separation of electrons and holes is obtained. The holes in the valence band of g-C_3N_4 oxidize H_2O molecules and generate $^{\cdot}OH$. The electrons in In_2S_3 conduction band are combined with O_2 to give strong superoxide ions ($^{\cdot}O_2^-$). RhB in aqueous solution reacts with these reactive redox agents and is degraded.

Although In_2S_3/ g-C_3N_4 heterojunction has previously been used to degrade textile dyes in effluents, herein the RFH based porous substrate has been used to stabilize and immobilize the photocatalyst that facilitates separation of the catalyst from solution and also reduces the band gap of the composite. Due to the presence of hydroxyl groups in RFH, this porous structure has the ability to adsorb rhodamine B as a cationic dye through electrostatic interactions, thus increasing the removing effect by adsorption.

CONCLUSION

A novel visible light heterogenic In_2S_3/ g-C_3N_4 in hydrogel photocatalyst was synthesized. The FTIR, DRS, XRD, BET, BJH, SEM, and EDX techniques were used to characterize chemical functional groups, optical properties, crystalline structure, the specific surface area of the porous hydrogel, size and volumes of pores, and morphology and chemical composition of samples, respectively. The addition of In_2S_3 and g-C_3N_4 increased the porosity of hydrogel. Porosity enhancement led to the more active sites and enhanced the efficiency of adsorption and finally improved the photocatalytic performance. By adding the nanomaterials to the hydrogel, the RhB adsorption percentage improved up to 10 times. The adsorption and photocatalytic progress of RhB in aqueous solution over In_2S_3/ g-C_3N_4 in hydrogel followed the first-order kinetic model and the rate constants were found to be 0.105 min^{-1} and 0.16 min^{-1}, respectively. Based on our results, In_2S_3/ g-C_3N_4 in hydrogel can be effectively and easily separated from the solution, and it could be a promising candidate for practical applications.

ACKNOWLEDGMENT

The authors wish to appreciate the Najafabad Branch, Islamic Azad University for partial support of this research.

CONFLICT OF INTERESTS

The authors declare that there is no conflict of interest regarding the publication of this manuscript.

REFERENCES

1. Fu J, Yu J, Jiang C, Cheng B. g-C3N4-Based Heterostructured Photocatalysts. Advanced Energy Materials. 2017;8(3):1701503.
2. Singh R, Kumar M, Tashi L, Khajuria H, Sheikh HN. Hydrothermal synthesis of nitrogen doped graphene supported cobalt ferrite (NG@CoFe2O4) as photocatalyst for the methylene blue dye degradation. Nanochemistry Research. 2018;3(2):149-59.
3. Deng Y, Feng C, Tang L, Zeng G, Chen Z, Zhang M. Nanohybrid Photocatalysts for Heavy Metal Pollutant Control. Nanohybrid and Nanoporous Materials for Aquatic Pollution Control: Elsevier; 2019. p. 125-53.
4. Wang Y, Wang X, Antonietti M. Polymeric Graphitic Carbon Nitride as a Heterogeneous Organocatalyst: From Photochemistry to Multipurpose Catalysis to Sustainable Chemistry. Angewandte Chemie International Edition. 2011;51(1):68-89.
5. Yan SC, Li ZS, Zou ZG. Photodegradation Performance of g-C3N4Fabricated by Directly Heating Melamine. Langmuir. 2009;25(17):10397-401.
6. Cao S, Yu J. g-C3N4-Based Photocatalysts for Hydrogen Generation. The Journal of Physical Chemistry Letters. 2014;5(12):2101-7.
7. Zheng Y, Liu J, Liang J, Jaroniec M, Qiao SZ. Graphitic carbon nitride materials: controllable synthesis and applications in fuel cells and photocatalysis. Energy & Environmental Science. 2012;5(5):6717.
8. Wang S, Li D, Sun C, Yang S, Guan Y, He H. Synthesis and characterization of g-C3N4/Ag3VO4 composites with significantly enhanced visible-light photocatalytic activity for triphenylmethane dye degradation. Applied Catalysis B: Environmental. 2014;144:885-92.
9. Xu H, Yan J, Xu Y, Song Y, Li H, Xia J, et al. Novel visible-light-driven AgX/graphite-like C3N4 (X=Br, I) hybrid materials with synergistic photocatalytic activity. Applied Catalysis B: Environmental. 2013;129:182-93.
10. Fan K, Jin Z, Yang H, Liu D, Hu H, Bi Y. Promotion of the excited electron transfer over Ni- and Co -sulfide co-doped g-C3N4 photocatalyst (g-C3N4/NixCo1−xS2) for hydrogen Production under visible light irradiation. Scientific Reports. 2017;7(1).
11. Fu J, Xu Q, Low J, Jiang C, Yu J. Ultrathin 2D/2D WO3/g-C3N4 step-scheme H2-production photocatalyst. Applied Catalysis B: Environmental. 2019;243:556-65.
12. Yuan Y-J, Shen Z, Wu S, Su Y, Pei L, Ji Z, et al. Liquid exfoliation of g-C3N4 nanosheets to construct 2D-2D MoS2/g-C3N4 photocatalyst for enhanced photocatalytic H2 production activity. Applied Catalysis B: Environmental.

2019;246:120-8.
13. Zhang M, Liu X, Zeng X, Wang M, Shen J, Liu R. Photocatalytic degradation of toluene by In2S3/g-C3N4 heterojunctions. Chemical Physics Letters: X. 2020;7:100049.
14. Kokane SB, Sasikala R, Phase DM, Sartale SD. In2S3 nanoparticles dispersed on g-C3N4 nanosheets: role of heterojunctions in photoinduced charge transfer and photoelectrochemical and photocatalytic performance. Journal of Materials Science. 2017;52(12):7077-90.
15. Fu X, Wang X, Chen Z, Zhang Z, Li Z, Leung DYC, et al. Photocatalytic performance of tetragonal and cubic β-In2S3 for the water splitting under visible light irradiation. Applied Catalysis B: Environmental. 2010;95(3-4):393-9.
16. He Y, Li D, Xiao G, Chen W, Chen Y, Sun M, et al. A New Application of Nanocrystal In2S3 in Efficient Degradation of Organic Pollutants under Visible Light Irradiation. The Journal of Physical Chemistry C. 2009;113(13):5254-62.
17. Liu G, Jiao X, Qin Z, Chen D. Solvothermal preparation and visible photocatalytic activity of polycrystalline β-In2S3nanotubes. CrystEngComm. 2011;13(1):182-7.
18. Xing C, Wu Z, Jiang D, Chen M. Hydrothermal synthesis of In 2 S 3 /g-C 3 N 4 heterojunctions with enhanced photocatalytic activity. Journal of Colloid and Interface Science. 2014;433:9-15.
19. Shafiee MRM, Parhizkar J, Radfar S. Removal of Rhodamine B by g-C3N4/Co3O4/MWCNT composite stabilized in hydrogel via the synergy of adsorption and photocatalysis under visible light. Journal of Materials Science: Materials in Electronics. 2019;30(13):12475-86.
20. Wang X, Liang Y, An W, Hu J, Zhu Y, Cui W. Removal of chromium (VI) by a self-regenerating and metal free g-C3N4/graphene hydrogel system via the synergy of adsorption and photo-catalysis under visible light. Applied Catalysis B: Environmental. 2017;219:53-62.
21. Ahmed EM. Hydrogel: Preparation, characterization, and applications: A review. Journal of Advanced Research. 2015;6(2):105-21.
22. Li H, Yin J, Meng Y, Liu S, Jiao T. Nickel/Cobalt-Containing polypyrrole hydrogel-derived approach for efficient ORR electrocatalyst. Colloids and Surfaces A: Physicochemical and Engineering Aspects. 2020;586:124221.
23. Hubert J, Plougonven E, Leonard A, Collin F. Study of the Drying Behavior of Resorcinol Formaldehyde Hydrogels: Experimental Investigation and Numerical Framework. Poromechanics VI; 2017/07/06: American Society of Civil Engineers; 2017.
24. Ghosh SK, Deguchi S, Mukai S-a, Tsujii K. Supercritical EthanolA Fascinating Dispersion Medium for Silica Nanoparticles. The Journal of Physical Chemistry B. 2007;111(28):8169-74.
25. Zhang Y, Pan Q, Chai G, Liang M, Dong G, Zhang Q, et al. Synthesis and luminescence mechanism of multicolor-emitting g-C3N4 nanopowders by low temperature thermal condensation of melamine. Scientific Reports. 2013;3(1).
26. Yamamoto T, Mukai SR, Nitta K, Tamon H, Endo A, Ohmori T, et al. Evaluation of porous structure of resorcinol-formaldehyde hydrogels by thermoporometry. Thermochimica Acta. 2005;439(1-2):74-9.
27. Fu J, Chang B, Tian Y, Xi F, Dong X. Novel C3N4–CdS composite photocatalysts with organic–inorganic heterojunctions: in situ synthesis, exceptional activity, high stability and photocatalytic mechanism. Journal of Materials Chemistry A. 2013;1(9):3083.
28. Ge L, Han C. Synthesis of MWNTs/g-C3N4 composite photocatalysts with efficient visible light photocatalytic hydrogen evolution activity. Applied Catalysis B: Environmental. 2012;117-118:268-74.
29. Huang NM. Synthesis and characterization of in 2S 3 nanorods in sucrose ester water-in-oil microemulsion. . Journal of Nanomaterials. 2011;2011:815709.
30. Liu L, Xiang W, Zhong J, Yang X, Liang X, Liu H, et al. Flowerlike cubic β-In2S3 microspheres: Synthesis and characterization. Journal of Alloys and Compounds. 2010;493(1-2):309-13.
31. Habibi MH, Parhizkar HJ. FTIR and UV–vis diffuse reflectance spectroscopy studies of the wet chemical (WC) route synthesized nano-structure CoFe2O4 from CoCl2 and FeCl3. Spectrochimica Acta Part A: Molecular and Biomolecular Spectroscopy. 2014;127:102-6.